PHYSICAL REVIEW D **86,** 094009 (2012)

Jet production in (un)polarized pp collisions: Dependence on jet algorithm

Asmita Mukherjee[1,2] and Werner Vogelsang[2]

[1]*Department of Physics, Indian Institute of Technology Bombay, Powai, Mumbai 400076, India*

[2]*Institute for Theoretical Physics, Tübingen University, Auf der Morgenstelle 14, Tübingen 72076, Germany*

(Received 9 September 2012; published 5 November 2012)

We investigate single-inclusive high-p_T jet production in longitudinally polarized pp collisions at the Relativistic Heavy Ion Collider, with particular focus on the algorithm adopted to define the jets. Following and extending earlier work in the literature, we treat the jets in the approximation that they are rather narrow, in which case analytical results for the corresponding next-to-leading order partonic cross sections can be obtained. This approximation is demonstrated to be very accurate for practically all relevant situations, even at Tevatron and LHC energies. We confront results for cross sections and spin asymmetries based on using cone and k_t-type jet algorithms. We find that jet cross sections at the Relativistic Heavy Ion Collider can differ significantly depending on the algorithm chosen, but that the spin asymmetries are rather robust. Our results are also useful for matching threshold-resummed calculations of jet cross sections to fixed-order ones.

DOI: 10.1103/PhysRevD.86.094009 PACS numbers: 12.38.Bx, 13.85.Ni, 13.88.+e

I. INTRODUCTION

Jets are copiously produced at high-energy hadron colliders. Among other things, they play important roles as precision probes of QCD and nucleon structure. At the Relativistic Heavy Ion Collider (RHIC), jets are by now a well-proven tool for investigating the spin structure of the nucleon through double-helicity asymmetries measured in the reaction $pp \to \text{jet}X$. The corresponding measurements [1] have in particular provided exciting information on the proton's polarized gluon distribution, Δg.

There is no unique way of defining a jet. As a result, different jet algorithms exist and are being used in experiments. The jet definitions and algorithms can be broadly divided into two classes [2]: (i) successive recombination algorithms [3–6], and (ii) cone algorithms [7]. For the former, one first defines a distance between a pair of produced objects (initially, two particles), as well as a *beam distance* of each object to the collider beam axis. For each object, the smallest of these distances is determined. If it is a beam distance, the object is called a jet and removed from the list of objects in the event; otherwise the two objects are combined into a single object. This procedure is repeated until no further recombinations take place. Prominent examples of successive recombination algorithms are the so-called k_t [3,4], Cambridge-Aachen [5], and anti-k_t [6] algorithms, which differ in how the distances are defined. We will collectively refer to such algorithms as "k_t-type" algorithms.

Cone algorithms also come in different variants [7]. They have in common that the jet is defined by the particles found inside a circle in the plane formed by rapidity and azimuthal angle, such that the sum of the four-momenta of these particles points in the direction of its center. While widely used in experiments, the traditional cone algorithms (notably the ones known as midpoint algorithm mostly used at RHIC [1,8] and the iterative cone algorithm) were found to be not infrared safe [9,10]. This evidently sets a serious limitation to the use of such algorithms in the theoretical calculation and to comparisons of data and theory. For single-inclusive jet cross sections, the lack of infrared safety becomes an issue first at next-to-next-to-leading order in perturbation theory, so that next-to-leading order (NLO) calculations remain meaningful in the sense that they produce finite and well-defined answers. In case of the midpoint cone algorithm, a solution to the problem of infrared unsafety was found in terms of the "seedless infrared-safe cone" (SISCone) algorithm [10]. It was also shown that the anti-k_t algorithm mentioned above can effectively cure the lack of infrared safety of the iterative cone algorithm [6]. As a result, the SISCone and all k_t-type algorithms are nowadays known to be infrared safe and are preferred for use in experiments.

In earlier work [11,12], the spin-dependent (and spin-averaged) cross sections for $pp \to \text{jet}X$ were derived at NLO. Reference [11] was based on a Monte Carlo integration approach, while [12] used a largely analytic technique for deriving the relevant partonic cross sections for cone algorithms, which becomes possible if one assumes the jet to be a rather narrow object [12–16]. This assumption is equivalent to the approximation that the cone opening R of the jet is not too large, and hence was termed *small cone approximation* (SCA) in Ref. [12]. In the SCA, one systematically expands the partonic cross sections around $R = 0$. The dependence on R is of the form $\mathcal{A}\log R + \mathcal{B} + \mathcal{O}(R^2)$. The coefficients $\mathcal{A}$ and $\mathcal{B}$ are retained and calculated analytically, whereas the remaining terms $\mathcal{O}(R^2)$ and beyond are neglected. The advantage of the analytical method is that it leads to much faster and more efficient computer codes and is hence readily suited for inclusion of jet spin asymmetry data from RHIC in a NLO global analysis of polarized parton distributions. Indeed, the results of Ref. [12] have been used in the global

analysis [17], where the experimental data from the STAR Collaboration [1] were used to constrain Δg. The SCA will of course fail if R becomes too large. It was shown in Ref. [12] that the SCA is in fact an excellent approximation to the full Monte Carlo calculation (which is valid for arbitrary cone openings), for all values of R and kinematics relevant at RHIC. (We shall revisit this finding in our phenomenological Sec. III below). At very small R, the SCA will technically remain accurate, but the NLO result will become physically unreliable. Ultimately, as $R \to 0$, the NLO cross section will change sign and nominally become negative. The reason for this behavior is that $|\log R|$ becomes very large. When this happens, logarithmic terms of the form $\alpha_s^k \log^k R$ that are present at higher orders in perturbation theory all become important and need to be taken into account to all orders. This resummation of terms $\alpha_s^k \log^k R$ will then tame the unphysical behavior of the NLO result. In practice, the NLO cross section turns negative at values of R well below 0.05 and hence not in a regime of interest for present experiments. A simple estimate based on comparing powers of $\alpha_s \log R$ indicates that the resummation of terms $\alpha_s^k \log^k R$ will likely not make any significant impact for $R \gtrsim 0.1$. We can therefore safely assume that our NLO predictions to be presented in this paper are reliable for R down to, at least, 0.2.

Commensurate with the procedure chosen by the STAR Collaboration, the calculation [12] was performed for the midpoint cone algorithm. In the present paper, we will extend the work in Ref. [12] to the case of k_t-type algorithms. We will again use the approximation of a rather narrow jet. As we do not really have a jet "cone" for the k_t-type algorithms, we shall from now on refer to this approximation as *narrow jet approximation* (NJA). This term will be collectively applied to both the cone (where it used to be the SCA) and the k_t-type algorithms. The meaning of the NJA will always be that the jet parameter R used to define the jet (cone opening for the cone algorithm and distance between two objects for the k_t-type algorithms) is not too large, as we shall discuss in more detail below.

One motivation for our new study is that k_t-type algorithms are also being considered by the STAR Collaboration now [18], so that it is timely to prepare the corresponding theoretical NLO calculations for the spin asymmetries. The differences between the jet cross sections for the cone and k_t-type algorithms in the NJA are also interesting from a theoretical point of view. We will find that they amount to finite contributions with leading order (LO) kinematics. As such they play a role as matching coefficients in threshold resummation studies of jet production, as was discussed in Ref. [19]. They also appear in a related context in studies of jet shapes in the framework of "soft collinear effective theories" [20].

The remainder of this paper is organized as follows: In Sec. II we present the technical details and analytical results of our calculation of single-inclusive jet cross sections in the NJA, focusing on the k_t-type algorithms. Section III contains phenomenological results relevant for RHIC. We summarize our work in Sec. IV.

II. TECHNICAL DETAILS

A. Cone and k_t-type jet definitions

We consider single-inclusive jet production in hadronic collisions, $pp \to \text{jet}X$, where the jet has a transverse momentum p_{T_J}, rapidity η_J, and azimuthal angle ϕ_J. The cross section is infinite unless a finite jet size is imposed as a parameter. The different jet algorithms vary in the way this size is defined. In the cone algorithm [7], one defines the jet by all particles j that satisfy

$$R_{jJ}^2 \equiv (\eta_J - \eta_j)^2 + (\phi_J - \phi_j)^2 \leq R^2. \tag{1}$$

Here η_j and ϕ_j denote the rapidities and azimuthal angles of the particle, and R is the jet cone aperture. The jet four-momentum sets the center of the cone; it is nowadays usually defined as the sum of the four-momenta of the particles j forming the jet.

For the k_t-type algorithms [3–6] one defines for each pair of objects (initially, particles) j, k the quantity

$$d_{jk} \equiv \min(k_{T_j}^{2p}, k_{T_k}^{2p}) \frac{R_{jk}^2}{R^2}, \tag{2}$$

where p is a parameter that specifies the algorithm, k_{T_j} denotes the transverse momentum of particle j with respect to the beam direction, and

$$R_{jk}^2 \equiv (\eta_j - \eta_k)^2 + (\phi_j - \phi_k)^2. \tag{3}$$

The parameter R is called the jet radius. d_{jk} may be viewed as a distance between two objects j and k. One also defines for each object a distance to the initial beams:

$$d_{jB} \equiv k_{T_j}^{2p}. \tag{4}$$

The algorithm identifies the smallest of the d_{jk} and d_{jB}. If it is a beam distance, the object is defined as a jet and removed from the list of objects. If the smallest distance is a d_{jk}, the two objects j, k are merged into a single one. The procedure is repeated until no objects are left in the event. As mentioned above, the jet algorithm is fully specified by the parameter p. We have $p = 1$ for the k_t algorithm [3,4], $p = 0$ for the Cambridge-Aachen algorithm [5], and $p = -1$ for the anti-k_t algorithm [6].

Note that on top of the choice of jet algorithm one also has to define how objects are to be merged if the need for that arises. Throughout this paper our choice will be (for both algorithms) to define the four-momentum of a new object as the sum of four-momenta of the partons that form the new object. This so-called "E recombination scheme" [7] is the most popular choice nowadays.

B. Calculation of single-inclusive jet production cross sections at NLO

The spin-averaged cross section for the process $p(P_a)p(P_b) \to \text{jet}(p_J)X$ can be written as [12]

$$\frac{d^2\sigma}{dp_{T_J}d\eta_J} = \frac{2p_{T_J}}{S}\sum_{a,b}\int_{VW}^{V}\frac{dv}{v(1-v)} \times \int_{VW/v}^{1}\frac{dw}{w}f_a(x_a,\mu_F)f_b(x_b,\mu_F) \times \left[\frac{d\hat{\sigma}^{(0)}_{ab\to\text{jet}X}(s,v)}{dv}\delta(1-w) + \frac{\alpha_s(\mu_R)}{\pi}\frac{d^2\hat{\sigma}^{(1)}_{ab\to\text{jet}X}(s,v,w,\mu_F,\mu_R;R)}{dvdw}\right], \quad (5)$$

where the dimensionless variables V and W are defined in terms of p_{T_J} and η_J as

$$V = 1 - \frac{p_{T_J}}{\sqrt{S}}e^{\eta_J} \quad \text{and} \quad W = \frac{p_{T_J}^2}{SV(1-V)}, \quad (6)$$

with $\sqrt{S} = \sqrt{(P_a + P_b)^2}$ the hadronic c.m.s. energy. v and w are the corresponding parton-level variables; they are given in terms of the partonic Mandelstam variables

$$s \equiv (p_a + p_b)^2, \qquad t \equiv (p_a - p_J)^2, \qquad u \equiv (p_b - p_J)^2, \quad (7)$$

as

$$v = 1 + \frac{t}{s}, \qquad w = \frac{-u}{s+t}. \quad (8)$$

The sum in (5) runs over all partonic channels $a + b \to \text{jet} + X$, with $d\hat{\sigma}^{(0)}_{ab\to\text{jet}X}$ and $d\hat{\sigma}^{(1)}_{ab\to\text{jet}X}$ the LO and NLO terms in the corresponding partonic cross sections, respectively. $f_a(x_a,\mu_F)$ and $f_b(x_b,\mu_F)$ denote the parton distribution functions at factorization scale μ_F whose partonic momentum fractions are determined by V, W, v, and w:

$$x_a = \frac{VW}{vw}, \qquad x_b = \frac{1-V}{1-v}. \quad (9)$$

Finally, μ_R in (5) is the renormalization scale for the strong coupling constant.

We note that expression (5) can be straightforwardly extended to the case of collisions of longitudinally polarized protons. Here one defines a spin-dependent cross section as

$$\frac{d^2\Delta\sigma}{dp_{T_J}d\eta_J} \equiv \frac{1}{2}\left[\frac{d^2\sigma^{++}}{dp_{T_J}d\eta_J} - \frac{d^2\sigma^{+-}}{dp_{T_J}d\eta_J}\right], \quad (10)$$

where the superscripts indicate the helicities of the colliding protons. The structure of Eq. (5) also applies to $d^2\Delta\sigma/dp_{T_J}d\eta_J$, except that the partonic cross sections and parton distribution functions are to be replaced by their spin-dependent counterparts $d\Delta\hat{\sigma}_{ab\to\text{jet}X}$ and $\Delta f_{a,b}(x_{a,b},\mu_F)$, respectively. The former are defined in analogy with (10), and for the latter we have

$$\Delta f_a(x,\mu_F) = f_a^+(x,\mu_F) - f_a^-(x,\mu_F), \quad (11)$$

where f_a^+ (f_a^-) denotes the distribution for partons of type a with the same (opposite) helicity as that of the parent proton. All our expressions below will be formulated for the spin-averaged case; however, they equally apply to the polarized case with the modifications just discussed.

A possible way of organizing the NLO calculation of the single-inclusive jet cross section was developed and employed in Refs. [12,14–16,21]. It starts from the NLO single-parton inclusive cross sections $d\hat{\sigma}_{ab\to cX}$, relevant for the single-inclusive hadron production process $pp \to hX$ and analytically known from previous calculations [15,22]. These cross sections cannot directly be used to describe jet production; they can, however, be converted to the desired single-inclusive jet cross sections. To this end, one first imagines a *jet cone* around the observed parton c and notices that a NLO single-parton inclusive cross section contains configurations where there is an additional parton d inside the cone (note that we use the term cone here just for simplicity—the considerations apply to any jet definition). For a jet cross section, the observed final state should not just be given by parton c, but by partons c and d jointly. One therefore subtracts these contributions and replaces them by terms for which partons c and d are both inside the cone and form the observed jet together. To be more precise, for a given partonic process $ab \to cde$ we have, after proper bookkeeping of all partonic configurations that are possible in the cone:

$$d\hat{\sigma}_{ab\to\text{jet}X} = [d\hat{\sigma}_c - d\hat{\sigma}_{c(d)} - d\hat{\sigma}_{c(e)}] + [d\hat{\sigma}_d - d\hat{\sigma}_{d(c)} - d\hat{\sigma}_{d(e)}] + [d\hat{\sigma}_e - d\hat{\sigma}_{e(c)} - d\hat{\sigma}_{e(d)}] + d\hat{\sigma}_{cd} + d\hat{\sigma}_{ce} + d\hat{\sigma}_{de}. \quad (12)$$

Here $d\hat{\sigma}_j$ is the single-parton inclusive cross section where parton j is observed (which also includes the virtual corrections), $d\hat{\sigma}_{j(k)}$ is the cross section where parton j is observed but parton k is also in the cone, and $d\hat{\sigma}_{jk}$ is the cross section when both partons j and k are inside the cone and jointly form the jet.

The single-parton inclusive cross sections $d\hat{\sigma}_j$ of Refs. [15,22] were obtained after a subtraction of final-state collinear singularities in the modified minimal subtraction ($\overline{\text{MS}}$) scheme. Upon calculation of the combinations $d\hat{\sigma}_{j(k)} + d\hat{\sigma}_{k(j)} - d\hat{\sigma}_{jk}$ in (12) one also finds collinear singularities, which must match those initially present in $(d\hat{\sigma}_j + d\hat{\sigma}_k)/2$. On the other hand, the full expression in Eq. (12), being an inclusive-jet cross section, must be collinear finite. Therefore, in order to obtain the combination in (12) correctly, one just needs to perform an

$\overline{\text{MS}}$ subtraction also of the singularities in the $d\hat{\sigma}_{j(k)} + d\hat{\sigma}_{k(j)} - d\hat{\sigma}_{jk}$. For further discussion, see Ref. [12].

In practice, it is convenient to consider the $d\hat{\sigma}_{j(k)}$ and $d\hat{\sigma}_{jk}$ separately. In the NJA, to which we will turn in the next subsection, they may in fact be computed analytically. At NLO, they both receive contributions only from real-emission $2 \to 3$ diagrams. Since for $d\hat{\sigma}_{j(k)}$ the jet is obtained from the single parton j, it is independent of the jet definition. The relevant results for this piece in the NJA may be found in Ref. [12]. For $d\hat{\sigma}_{jk}$, on the other hand, the situation is different since here both particles j and k jointly form the jet. In Refs. [12,14,16] the $d\hat{\sigma}_{jk}$ were obtained for the case of cone algorithms. In the following we will derive them also for the k_t-type algorithms, using again the NJA.

C. Calculation of $d\hat{\sigma}_{jk}$ in the "narrow jet approximation"

It is instructive to discuss the cone and k_t-type algorithms in parallel, in order to make contact with the derivations made in Ref. [12] and to make our paper self-contained. From Sec. II A, we see that both the cone and the k_t-type algorithms contain a jet parameter R. In the NJA one assumes R to be relatively small. As discussed at the end of Sec. II A, our choice is to merge objects by adding their four-momenta. For $d\hat{\sigma}_{jk}$ this means that the four-momentum p_J of the jet is the sum of the parton four-momenta p_j and p_k.

We first observe that for the k_t-type algorithms the two partons j, k are merged into one jet if their distance defined in (2) is smaller than their respective beam distances d_{iB} and d_{jB} defined in (4). For $d\hat{\sigma}_{jk}$ this has to be the case by definition, and we therefore arrive at the condition

$$R_{jk}^2 \leq R^2 \quad \text{for } k_t - \text{type algorithms}, \tag{13}$$

with R_{ij} defined in Eq. (3). We stress that this condition holds for *all* k_t-type algorithms, regardless of the choice of the parameter p. This implies that at NLO all k_t-type algorithms lead to the same jet cross section, a result that does not rely on the NJA. Equation (13) is to be contrasted with Eq. (1) valid for the cone algorithm:

$$R_{jJ}^2 \leq R^2 \wedge R_{kJ}^2 \leq R^2 \quad \text{for cone algorithm}. \tag{14}$$

The difference between Eqs. (13) and (14) is solely responsible for any differences between the NLO results for the two types of jet algorithms. For the k_t-type algorithms it is the *distance* between the two partons that is constrained by the jet algorithm, whereas for the cone algorithm it is the distance of each parton to the jet itself. Note that this observation was already made in Ref. [3], and in Ref. [20] in a slightly different context.

As was shown in Ref. [12], in the NJA $d\hat{\sigma}_{jk}$ is, up to trivial factors, given by the following expression [see Eqs. (19), (20), and (27) of that paper]:

$$\frac{d\hat{\sigma}_{jk}}{dvdw} \propto \int \frac{dPS_3}{dvdw} \frac{P_{jK}^{<}(z)}{2p_j \cdot p_k}, \tag{15}$$

where the integration dPS_3 is over the phase space of the three-body final state of the overall partonic process, which is carried out in $d = 4 - 2\varepsilon$ dimensions. Expression (15) arises from the fact that $d\hat{\sigma}_{jk}$ is strongly dominated by contributions for which particles j and k result from collinear splitting of an intermediate particle K. The reason is that in this case the propagator of the intermediate particle, represented by the denominator $1/(2p_j \cdot p_k)$, goes on shell. For instance, if the jet is formed by a quark and a gluon, the pair will predominantly originate from a quark splitting into a quark plus a gluon, described by the splitting functions P_{qq} and P_{gq}. The argument z of the splitting function is the fraction of the intermediate particle's momentum transferred in the splitting. The superscript "$<$" on the splitting function indicates that the d-dimensional splitting function $P_{jK}(z)$ is strictly at $z < 1$, that is, without its $\delta(1-z)$ contribution that is present when $j = K$. This is a necessary condition in order to have two partons producing the jet. Explicitly, we have

$$\begin{aligned}
P_{qq}^{<}(z) &= C_F\left[\frac{1+z^2}{1-z} - \varepsilon(1-z)\right],\\
P_{qg}^{<}(z) &= \frac{1}{2}[z^2 + (1-z)^2 - 2\varepsilon z(1-z)],\\
P_{gq}^{<}(z) &= C_F\left[\frac{1+(1-z)^2}{z} - \varepsilon z\right],\\
P_{gg}^{<}(z) &= 2C_A\frac{(1-z+z^2)^2}{z(1-z)},
\end{aligned} \tag{16}$$

with $C_A = 3$ and $C_F = 4/3$ the usual SU(3) Casimir operators. For additional details, we refer the reader to Ref. [12].

Making use of the fact that $p_J = p_j + p_k$, the term on the right-hand side of (15) may be written as [12]

$$\begin{aligned}
&\int \frac{dPS_3}{dvdw}\frac{P_{jK}^{<}(z)}{(2p_j\cdot p_k)}\\
&= \left[\frac{1}{8\pi}\left(\frac{4\pi}{s}\right)^{\varepsilon}\frac{(v(1-v))^{-\varepsilon}}{\Gamma(1-\varepsilon)}\right]\frac{1}{8\pi^2}\left(\frac{4\pi}{s}\right)^{\varepsilon}\frac{\delta(1-w)}{\Gamma(1-\varepsilon)}\\
&\quad\times\int_0^{E_J} dE_j \frac{E_J}{E_k^2}\left(\frac{E_j^2}{s}\right)^{-\varepsilon} P_{jK}^{<}(z)\int_0^{\theta_{\max}} d\theta_j \frac{\sin^{1-2\varepsilon}\theta_j}{1-\cos\theta_{jk}},
\end{aligned} \tag{17}$$

where $E_J = E_j + E_k$ is the jet energy (with $E_{j,k}$ the energies of partons j, k), $z = E_j/E_J$, and θ_{jk} the angle between the three-momenta of partons j and k. θ_j is the polar angle of parton j, measured with respect to the jet direction. $\theta_{\max}$ is an upper limit on the θ_j integration that needs to be derived according to the jet algorithm. It is of the order of the jet parameter R, and hence treated as small in the NJA.

It is useful to write the θ_j integral as an integral over the (squared) invariant mass $p_J^2 \equiv m^2 = 2p_j \cdot p_k$ of the produced jet. One finds

$$\cos(\theta_{jk}) = 1 - \frac{m^2}{2E_jE_k}, \quad \cos(\theta_j) = \frac{2E_jE_J - m^2}{2E_j\sqrt{E_J^2 - m^2}}. \tag{18}$$

With this one obtains after some algebra:

$$\int \frac{dPS_3}{dvdw}\frac{P_{jK}^<(z)}{(2p_j\cdot p_k)} = \left[\frac{1}{64\pi^3}\left(\frac{4\pi}{\sqrt{s}}\right)^{2\varepsilon}\frac{(v(1-v))^{-\varepsilon}}{\Gamma^2(1-\varepsilon)}\right]\delta(1-w) \times \int_0^1 dz z^{-\varepsilon}(1-z)^{-\varepsilon}P_{jK}^<(z)\int_0^{m^2_{\max}}\frac{dm^2}{m^2}m^{-2\varepsilon}, \tag{19}$$

where we have also expressed the integral over the energy E_j as an integral over z. In the NJA, m^2 is a small quantity, and we have hence neglected powers of m^2 wherever possible. Note however that the m^2 integral produces a $1/\varepsilon$ singularity at the lower end.

All that is left to be done now is to determine the upper limit of the integral over m^2, which depends on the jet algorithm chosen. In order to make contact with the results in Ref. [12], we do this first for the cone algorithms and afterwards for the k_t-type algorithms we are mainly interested in here. In both cases we first write the jet four-momentum as

$$p_J = \left(E_J, |\vec{p}_J|\frac{\cos(\phi_J)}{\cosh(\eta_J)}, |\vec{p}_J|\frac{\sin(\phi_J)}{\cosh(\eta_J)}, |\vec{p}_J|\tanh(\eta_J)\right), \tag{20}$$

where

$$|\vec{p}_J| = \sqrt{E_J^2 - m^2}. \tag{21}$$

For the parton momenta p_j and p_k, which are lightlike, we write accordingly

$$p_j = E_j\left(1, \frac{\cos(\phi_j)}{\cosh(\eta_j)}, \frac{\sin(\phi_j)}{\cosh(\eta_j)}, \tanh(\eta_j)\right), \quad p_k = E_k\left(1, \frac{\cos(\phi_k)}{\cosh(\eta_k)}, \frac{\sin(\phi_k)}{\cosh(\eta_k)}, \tanh(\eta_k)\right), \tag{22}$$

with the azimuthal angles $\phi_{j,k}$ and pseudorapidities $\eta_{j,k}$ of the partons.

(i) Cone algorithms: We write

$$m^2 = 2p_j\cdot p_k = 2p_j\cdot p_J \approx 2E_jE_J\frac{\cosh(\eta_j-\eta_J)-\cos(\phi_j-\phi_J)}{\cosh(\eta_j)\cosh(\eta_J)} + \frac{E_jm^2}{E_J}\frac{\cos(\phi_j-\phi_J)+\sinh(\eta_j)\sinh(\eta_J)}{\cosh(\eta_j)\cosh(\eta_J)}, \tag{23}$$

where we have expanded $|\vec{p}_J|$ to first order in m^2. The combination $(\cosh(\eta_j-\eta_J)-\cos(\phi_j-\phi_J))$ in (23) is small, while in the other term m^2 is small. Therefore, to the order we consider, we can set $\eta_j = \eta_J$, $\phi_j = \phi_J$ in all other places. This gives

$$m^2 \approx \frac{E_jE_J}{\cosh^2(\eta_J)}R_{jJ}^2 + \frac{E_jm^2}{E_J}, \tag{24}$$

where R_{jJ} is as defined in Eq. (1). We solve for m^2 and get

$$m^2 \approx \frac{E_J^2}{\cosh^2(\eta_J)}\frac{z}{1-z}R_{jJ}^2. \tag{25}$$

Likewise, we find

$$m^2 \approx \frac{E_J^2}{\cosh^2(\eta_J)}\frac{1-z}{z}R_{kJ}^2. \tag{26}$$

The jet criterion (14) in the cone algorithm then immediately translates into

$$m^2_{\max,\text{cone}} = \frac{E_J^2R^2}{\cosh^2(\eta_J)}\min\left(\frac{z}{1-z}, \frac{1-z}{z}\right). \tag{27}$$

The last two integrals in (19) are now readily performed:

$$\int_0^1 dz z^{-\varepsilon}(1-z)^{-\varepsilon}P_{jK}^<(z)\int_0^{m^2_{\max,\text{cone}}}\frac{dm^2}{m^2}m^{-2\varepsilon} = -\frac{1}{\varepsilon}\left(\frac{E_J^2R^2}{\cosh^2(\eta_J)}\right)^{-\varepsilon}I_{jK}^{\text{cone}}, \tag{28}$$

where

$$I_{jK}^{\text{cone}} \equiv \left[\int_0^{1/2}dz z^{-2\varepsilon} + \int_{1/2}^1 dz(1-z)^{-2\varepsilon}\right]P_{jK}^<(z). \tag{29}$$

The explicit results for these integrals for the various splitting functions in (16) were given in [12]:

$$I_{qq}^{\text{cone}} = C_F\left[-\frac{1}{\varepsilon}-\frac{3}{2}+\varepsilon\left(-\frac{7}{2}+\frac{\pi^2}{3}-3\log 2\right)\right] = I_{gq}^{\text{cone}},$$
$$I_{qg}^{\text{cone}} = \frac{1}{2}\left[\frac{2}{3}+\varepsilon\left(\frac{23}{18}+\frac{4}{3}\log 2\right)\right],$$
$$I_{gg}^{\text{cone}} = 2C_A\left[-\frac{1}{\varepsilon}-\frac{11}{6}+\varepsilon\left(-\frac{137}{36}+\frac{\pi^2}{3}-\frac{11}{3}\log 2\right)\right]. \tag{30}$$

Note that the ratio $R/\cosh(\eta_J)$ corresponds to the half-opening δ of the jet cone considered in Ref. [12]. We also note the logarithmic dependence of $d\hat{\sigma}_{jk}$ on R arising from the factor $R^{-2\varepsilon}$ in Eq. (28). At first sight, Eq. (28) would also suggest the presence of double-logarithmic terms $\propto \log^2 R$ in the jet cross section, resulting from the double poles $\propto 1/\varepsilon^2$ that are generated in the diagonal cases $j = K$. These double logarithms cancel, however, against similar terms in the piece $d\hat{\sigma}_{j(k)} + d\hat{\sigma}_{k(j)}$ defined in Eq. (12) [13]. This cancellation happens simultaneously with that of the double poles between $d\hat{\sigma}_{jk}$ and $d\hat{\sigma}_{j(k)} + d\hat{\sigma}_{k(j)}$.

(ii) k_t-type algorithms: Here we use Eq. (22) to directly compute

$$m^2 = \frac{2E_jE_k}{\cosh(\eta_j)\cosh(\eta_k)}(\cosh(\eta_j-\eta_k)-\cos(\phi_j-\phi_k)). \tag{31}$$

We can approximate this by

$$\begin{aligned} m^2 &\approx \frac{E_jE_k}{\cosh^2(\eta_J)}((\eta_j-\eta_k)^2+(\phi_j-\phi_k)^2) \\ &= \frac{E_jE_k}{\cosh^2(\eta_J)}R_{jk}^2, \end{aligned} \tag{32}$$

with R_{jk} defined in (13). The condition $R_{jk}^2 \leq R^2$ then immediately gives

$$m^2_{\max,k_t} = \frac{E_J^2R^2}{\cosh^2(\eta_J)}z(1-z), \tag{33}$$

and instead of (28) we have

$$\begin{aligned} &\int_0^1 dz z^{-\varepsilon}(1-z)^{-\varepsilon}P_{jK}^{<}(z)\int_0^{m^2_{\max,k_t}}\frac{dm^2}{m^2}m^{-2\varepsilon} \\ &\quad = -\frac{1}{\varepsilon}\left(\frac{E_J^2R^2}{\cosh^2(\eta_J)}\right)^{-\varepsilon}I_{jK}^{k_t}, \end{aligned} \tag{34}$$

where

$$I_{jK}^{k_t} \equiv \int_0^1 dz[z(1-z)]^{-2\varepsilon}P_{jK}^{<}(z), \tag{35}$$

which, using (16), gives

$$\begin{aligned} I_{qq}^{k_t} &= C_F\left[-\frac{1}{\varepsilon}-\frac{3}{2}+\varepsilon\left(-\frac{13}{2}+\frac{2\pi^2}{3}\right)\right] = I_{gq}^{k_t}, \\ I_{qg}^{k_t} &= \frac{1}{2}\left[\frac{2}{3}+\frac{23}{9}\varepsilon\right], \\ I_{gg}^{k_t} &= 2C_A\left[-\frac{1}{\varepsilon}-\frac{11}{6}+\varepsilon\left(-\frac{67}{9}+\frac{2\pi^2}{3}\right)\right]. \end{aligned} \tag{36}$$

Comparison with (30) shows that the pole terms in Eqs. (28) and (34) are the same, as they have to be. The finite remainders, however, differ and will lead to finite and R-independent differences in the NLO cross sections for the two types of algorithms. As seen from Eq. (17), the cross sections $d\hat{\sigma}_{jk}$ are proportional to $\delta(1-w)$ and hence have LO kinematics. This will, therefore, also be true for the finite differences just mentioned. We note that expressions similar to those in (36) were also obtained in Ref. [20] in the context of jet studies in soft collinear effective theories.

It is now straightforward to use the integrals $I_{jK}^{k_t}$ given above to derive the NLO jet cross section for the k_t-type algorithms in the NJA—the calculation proceeds exactly as in Ref. [12]. In fact, it is very easy to change the numerical code of Jäger *et al.* [12] to the case of the k_t-type algorithms: The integrals I_{jK}^{cone} are the only sources of terms $\propto \log 2$ in the NLO calculation for the cone algorithms. Thus, by replacing these terms appropriately in each subprocess one can translate the result from the cone algorithm to the case of k_t-type algorithms without having to do the full calculation in (12).

While we have derived all the results above for the spin-averaged cross section, it is straightforward to extend them to the case of jet production in polarized collisions. In the NJA, the contributions by particles j and k forming the jet entirely arise from *final-state* emission, which is independent of the polarization of the initial partons. Therefore the same integrals I_{jK}^{cone} or $I_{jK}^{k_t}$ apply to the polarized case.

III. PHENOMENOLOGICAL RESULTS

In this section, we present some phenomenological results for single-inclusive jet production cross sections and spin asymmetries in pp collisions at RHIC. Our main focus is of course on the sensitivity of these quantities to the jet algorithm used.

A. Unpolarized collisions

We begin by ascertaining the accuracy of the NJA. It was shown already in Ref. [12] that for the cone algorithm the approximation is very accurate for the values of R and kinematics relevant at RHIC. To confirm this finding, we make use of the recently developed fastNLO package [23] which is based on the NLO code NLOJet++ by Nagy [24] and allows us to compute NLO jet cross sections with Monte Carlo integration methods. In fact, the authors of the code offer an online tool that provides numbers for the jet cross section at RHIC for the midpoint cone algorithm, as used by the STAR Collaboration [1]. In the upper left part of Fig. 1 we compare these results to the ones we find with our code based on the NJA. We plot the ratio of the two theoretical results. We have used here the CTEQ6.6M parton distributions [25], which will be our choice for the spin-averaged parton distribution functions throughout this paper. The comparison is for $\sqrt{S} = 200$ GeV, $R = 0.4$, and a range of rapidity $0.2 \leq |\eta_J| \leq 0.8$. We have chosen the factorization and renormalization scales as $\mu_F = \mu_R = p_{T_J}$. As one can see, there is excellent agreement between the full NLO Monte Carlo calculation and our approximated result. The largest deviations occur at the lowest p_{T_J}; even here they amount to at most 5%.

The lower left part of Fig. 1 shows a similar comparison for the k_t-type algorithms (we remind the reader that at NLO the jet cross section is the same for all k_t-type algorithms). The exact NLO calculation was performed here with the FastJet code [26,27], which is also based on Ref. [24]. Kinematics are similar as before, except that we have used here the rapidity range $|\eta_J| \leq 0.6$. We have again used $R = 0.4$ for the jet parameter in the k_t-type algorithms. Again, the NJA reproduces the full NLO calculation very accurately. Interestingly, comparing the upper and lower left parts of Fig. 1, we observe that the NJA very slightly overpredicts the NLO cross section for the case of cone algorithms, but underpredicts it in the

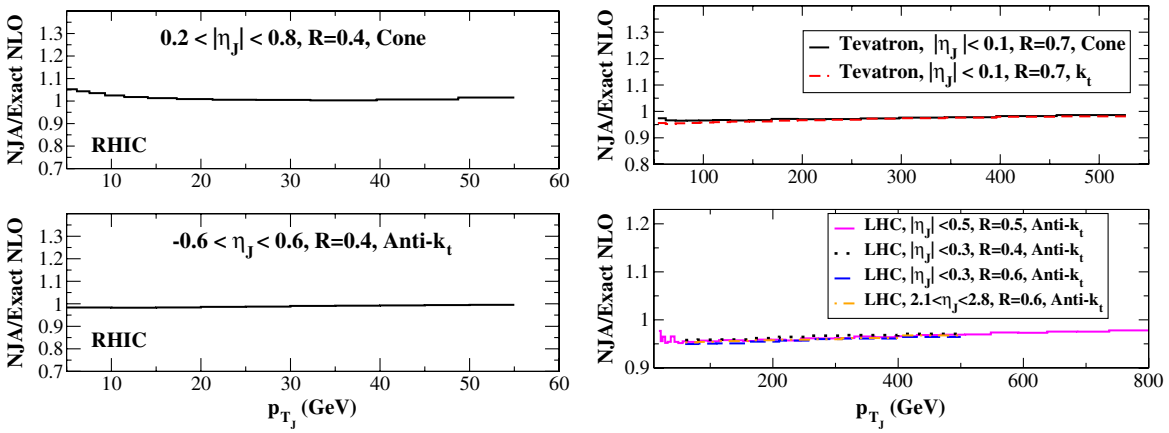

FIG. 1 (color online). Upper left: Ratio of single-inclusive jet cross sections at RHIC for the cone algorithm, as computed within the NJA and with fastNLO [23]. Lower left: Same for the jet cross sections for the k_t-type algorithms. Here, the exact NLO calculation was performed with the FastJet code [26,27]. Right: Similar comparisons for Tevatron (upper, $\sqrt{S} = 1960$ GeV) and LHC (lower, $\sqrt{S} = 7$ TeV) energies. The exact NLO results for Tevatron and for the LHC with $R = 0.5$ were obtained from fastNLO, the others from FastJet.

k_t-type case. We note that the excellent overall agreement between the NJA and the exact NLO calculation occurs also for other choices of the factorization and renormalization scales.

As an aside, we also show in the right part of Fig. 1 results for similar comparisons for $p\bar{p}$ collisions at the Tevatron ($\sqrt{S} = 1960$ GeV) and for the LHC ($\sqrt{S} = 7$ TeV), for various jet algorithms. The kinematics correspond to those used in experiments [28–31]. The exact NLO results were again obtained using the fastNLO [23] and FastJet [26,27] packages. One can see that the NJA also works very well in these cases.

Another way of gauging the accuracy of the NJA is to consider the ratio of jet cross sections for different jet parameters R:

$$\mathcal{R}(R_1, R_2) \equiv \frac{d^2\sigma/dp_{T_J}d\eta_J(R = R_1)}{d^2\sigma/dp_{T_J}d\eta_J(R = R_2)}. \qquad (37)$$

As shown in Ref. [32], $\mathcal{R}$ can be expanded perturbatively in orders of α_s. To the lowest nontrivial order one has

$$\mathcal{R}(R_1, R_2) = 1 + \frac{d^2\sigma^{\mathrm{NLO}}(R_1) - d^2\sigma^{\mathrm{NLO}}(R_2)}{d^2\sigma^{\mathrm{NLO}}|_{\mathcal{O}(\alpha_s^2)}}, \qquad (38)$$

where $d^2\sigma^{\mathrm{NLO}}(R)$ denotes the NLO cross section for a given R and $d^2\sigma^{\mathrm{NLO}}|_{\mathcal{O}(\alpha_s^2)}$ its truncation to the lowest order, keeping however the strong coupling constant α_s and the parton distributions at NLO. $d^2\sigma^{\mathrm{NLO}}|_{\mathcal{O}(\alpha_s^2)}$ does not depend on R. The difference of cross sections in the numerator of (38) is of order α_s^3, so that $\mathcal{R}(R_1, R_2)$ is of the form $1 + \mathcal{O}(\alpha_s)$. Figure 2 shows the result for $\mathcal{R}(0.2, 0.4)$ at RHIC energy $\sqrt{S} = 200$ GeV, as a function of p_{T_J}. The cross sections have been integrated over $|\eta_J| \leq 0.6$, and we have used here scales $\mu_F = \mu_R = p_{T_J}$. Our result may be directly compared to the corresponding one given in Ref. [32] for the same set of parameters, also shown in the figure, where the full FastJet code was used. One can see that the agreement is excellent, impressively demonstrating the accuracy of the NJA. We note, however, that in the NJA the ratio $\mathcal{R}(R_1, R_2)$ is independent of the jet algorithm chosen. The agreement seen in Fig. 2 hence is a test of the NJA as such, but not of the implementation of a specific jet algorithm.

Having established the validity of the NJA, we now provide results for jet cross sections at RHIC. Figure 3 shows the spin-averaged cross sections for $|\eta_J| \leq 1$ at $\sqrt{S} = 200$ GeV (left) and $\sqrt{S} = 500$ GeV (right). Results are presented for both the cone and the k_t-type algorithms, using two values for the jet parameter, $R = 0.4$ and $R = 0.7$. The renormalization and factorization scales have again been set to p_{T_J}. Figure 4 examines how the cross sections vary with

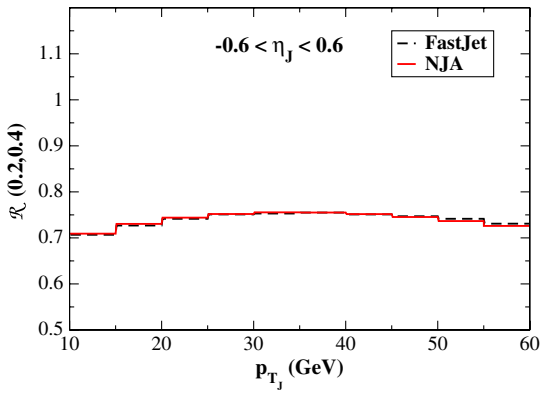

FIG. 2 (color online). The ratio $\mathcal{R}(0.2, 0.4)$ as defined in Eq. (38) for pp collisions at RHIC at $\sqrt{S} = 200$ GeV. The solid histogram shows our result within the NJA, while the dashed one shows the corresponding result for the k_t/anti-k_t algorithms presented in Ref. [32].

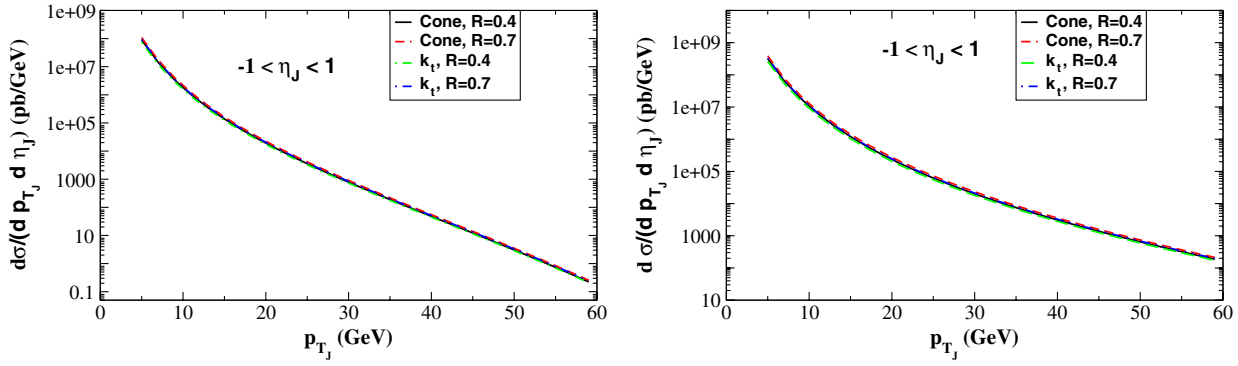

FIG. 3 (color online). Spin-averaged NLO cross sections for single-inclusive jet production at RHIC at center-of-mass energies 200 GeV (left) and 500 GeV (right). Results are shown for the cone and k_t-type algorithms, for two different values of the jet parameter R.

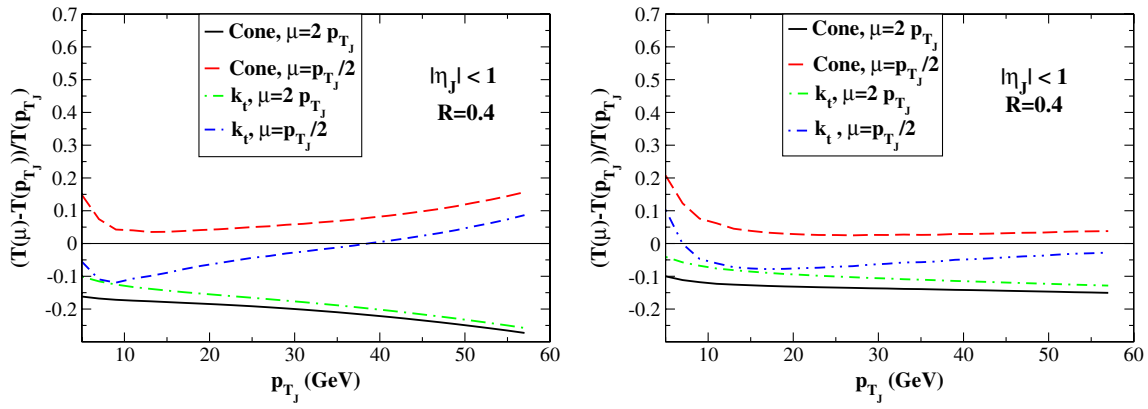

FIG. 4 (color online). Scale dependence of the NLO cross sections shown in Fig. 3 for $R = 0.4$ for center-of-mass energies 200 GeV (left) and 500 GeV (right). For notational convenience we have defined $T(\mu) \equiv d^2\sigma/dp_{T_J}d\eta_J$ at a given scale $\mu = \mu_F = \mu_R$.

the choice for the scale $\mu \equiv \mu_F = \mu_R$, for the case $R = 0.4$. We vary the scales in the region $p_{T_J}/2 \leq \mu \leq 2p_{T_J}$ and show the relative deviation from the result for the case $\mu = p_{T_J}$. Interestingly, for this value of R, the scale dependence is not too similar for the cone and the k_t-type algorithms. For the former, the cross section increases monotonically when going from scale $\mu = 2p_{T_J}$ to $\mu = p_{T_J}/2$, while for the latter the cross section for $\mu = p_{T_J}$ is for most p_{T_J} larger than those for both other scales. Also, the scale dependence is overall somewhat smaller for the k_t-type algorithms. We have verified that these patterns are present in the exact NLO calculation with FastJet [27].

We now turn to a more detailed comparison of the jet cross sections at RHIC for the two different jet algorithms. We define the ratio

$$\mathcal{R}_{\text{algo}} \equiv \frac{[d^2(\Delta)\sigma/dp_{T_J}d\eta_J]_{k_t-\text{type}}}{[d^2(\Delta)\sigma/dp_{T_J}d\eta_J]_{\text{cone}}}, \tag{39}$$

choosing the same jet parameter R for both cross sections. Figure 5 shows our results for $\mathcal{R}_{\text{algo}}$ as a function of p_{T_J} (we have chosen p_{T_J} bins of 5 GeV width), for $R = 0.4$ and 0.7. We present results for both energies relevant at RHIC, $\sqrt{S} = 200$ GeV (left) and $\sqrt{S} = 500$ GeV (right). We have in both cases integrated the cross sections over the rapidity range $|\eta_J| \leq 1$. Results are presented for the default scale $\mu = p_{T_J}$. As one can see, for this scale, the cross section for the k_t-type algorithms is about 10% smaller than that for the cone algorithm, except at $p_{T_J} \lesssim 10$ GeV where the ratio $\mathcal{R}_{\text{algo}}$ drops more strongly. Our results are consistent with the trend seen in jet algorithm studies by the STAR Collaboration [33]. The ratio $\mathcal{R}_{\text{algo}}$ also shows relatively little dependence on the jet parameter R. Keeping in mind the results shown in Fig. 4, it is clear that the scale dependence of $\mathcal{R}_{\text{algo}}$ must be quite large. As an example, the dash-dotted lines in the left part of Fig. 5 show $\mathcal{R}_{\text{algo}}$ at $\sqrt{S} = 200$ GeV and $R = 0.4$ computed for scales $\mu = p_{T_J}/2$ (lower curve) and $\mu = 2p_{T_J}$ (upper curve). Indeed, $\mathcal{R}_{\text{algo}}$ depends quite sensitively on μ. However, the basic finding that the jet cross section for the k_t-type algorithms is smaller than that for the cone algorithm for the same value of R is independent of the scale choice. This observation in fact implies that a choice of a *larger* R for the k_t-type algorithms should bring the two cross sections much closer together. Indeed, it was

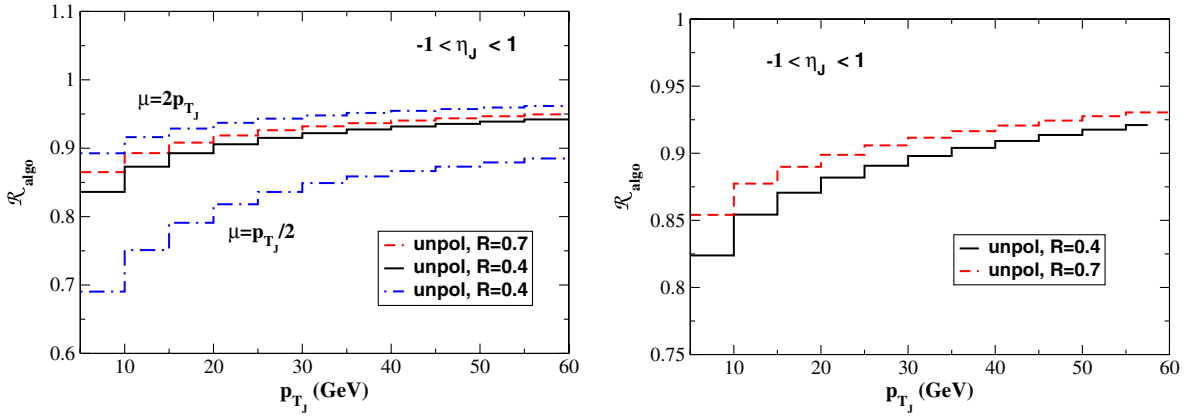

FIG. 5 (color online). The ratio $\mathcal{R}_{\rm algo}$ at RHIC for $\sqrt{S} = 200$ GeV (left) and $\sqrt{S} = 500$ GeV (right), for the spin-averaged case. Results are shown for two different values of the jet parameter R. We have chosen the scale $\mu = p_{T_J}$ everywhere, except for the case $\sqrt{S} = 200$ GeV, $R = 0.4$, where the dash-dotted lines also show the results for $\mu = p_{T_J}/2$ (lower) and $\mu = 2p_{T_J}$ (upper).

found in Ref. [3] that a choice $R_{k_t} \approx 1.35R_{\rm cone}$ makes the cross sections for the two algorithms quite similar, also for other choices of the scale μ. We confirm this finding.

B. Longitudinally polarized collisions

For the polarized case we use the "DSSV" helicity parton distributions of Ref. [17]. Our first finding is that for the polarized case the effects of changing the jet algorithm are somewhat more pronounced than in the unpolarized one. Figure 6 shows the ratio $\mathcal{R}_{\rm algo}$ for polarized collisions at RHIC, again computed for the scale $\mu = p_{T_J}$. $\mathcal{R}_{\rm algo}$ is again around 90% at high p_{T_J}, but shows large deviations from unity in the bin around $p_{T_J} = 12.5$ GeV. The reason for this is that for the DSSV set of parton distributions the polarized jet cross section crosses zero around $p_{T_J} = 10$ GeV. Depending on the jet algorithm, this zero will be at slightly different locations, making the denominator and numerator of $\mathcal{R}_{\rm algo}$ vastly different there. This is, of course, for the most part an artifact of the way we are performing the comparison of the jet cross sections, taking ratios of small numbers at some $p_{T_J} \sim 10$ GeV. On the other hand, it does demonstrate the issue that in regions where the polarized cross section is very small it may also be quite susceptible to the choice of jet algorithm and hence (at the nonperturbative level) to hadronization corrections. We note that the difference between the cross sections for the k_t-type and cone algorithms may again be diminished by choosing a larger value of R for the former, $R_{k_t} \approx 1.35R_{\rm cone}$ as in the spin-averaged case discussed above. This also brings the two polarized cross sections somewhat closer together in the bins near their zero, even though marked differences remain here.

Figure 7 shows the spin asymmetries A_{LL} at RHIC, which are defined by

$$A_{LL} \equiv \frac{d^2\Delta\sigma/dp_{T_J}d\eta_J}{d^2\sigma/dp_{T_J}d\eta_J}. \tag{40}$$

For the denominator we use the spin-averaged cross sections shown in Fig. 3. The most important observation is that the asymmetries are quite insensitive to the jet algorithm chosen, and also to the value of the jet parameter R. The exceptions are of course regions where the polarized cross

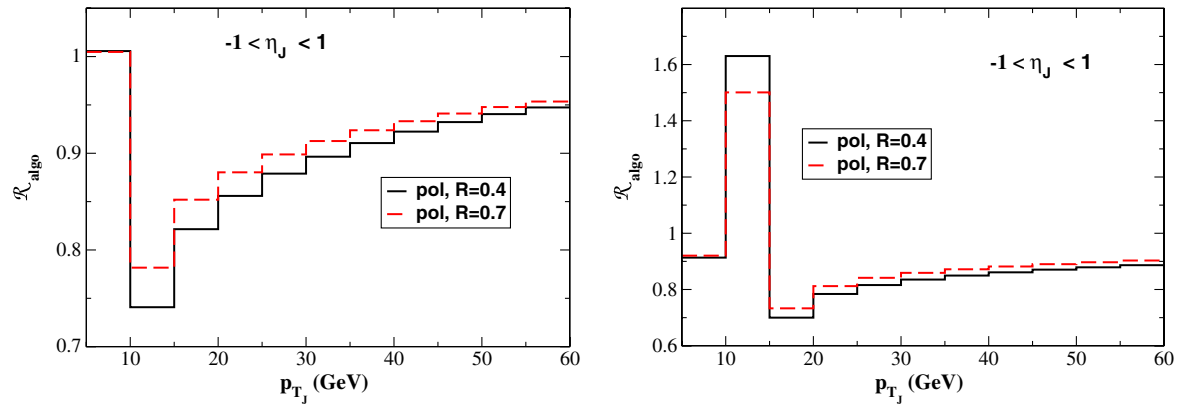

FIG. 6 (color online). Same as Fig. 5, but for the spin-dependent case.

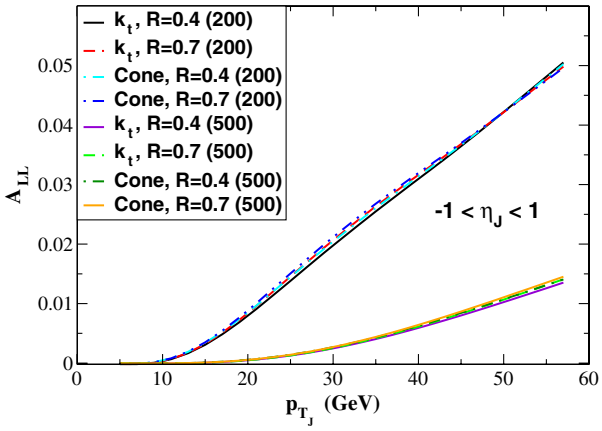

FIG. 7 (color online). Double-longitudinal spin asymmetries A_{LL} at RHIC, for $\sqrt{S} = 200$ GeV and $\sqrt{S} = 500$ GeV and various jet definitions. We have averaged over $|\eta_J| \leq 1$. The scales have been chosen as $\mu_F = \mu_R = p_{T_J}$.

section (nearly) vanishes, as we saw in Fig. 6. In these regions, A_{LL} is very small, and so these exceptions are not really noticeable in Fig. 7.

V. CONCLUSIONS

We have computed the NLO cross sections for single-inclusive high-p_T jet production in spin-averaged and longitudinally polarized pp collisions at RHIC, with special focus on the algorithm adopted to define the jets. Following Ref. [12], we have treated the jets in the approximation that they are rather narrow (*narrow jet approximation*). In this approximation one can derive analytical results for the corresponding partonic cross sections, which are of the form $\mathcal{A}\log R + \mathcal{B}$ with R the jet parameter. We have extended the results of Ref. [12] to the case where an infrared-safe "k_t-type" algorithm (k_t, anti-k_t, Cambridge-Aachen algorithm) is used. By comparison to available "exact" NLO jet codes for spin-averaged scattering [23,26], we have found that the narrow jet approximation is very accurate at RHIC for practically all relevant situations. The same is true even at Tevatron and LHC energies.

Our numerical results show that for given R, jet cross sections at RHIC depend significantly on the algorithm chosen. Moreover, the scale dependence of the cross sections can be quite different for cone and k_t-type algorithms. For polarized cross sections, the dependence on the jet algorithm can be very pronounced in the vicinity of a zero of the cross section. On the other hand, spin asymmetries at RHIC overall turn out to be quite robust with respect to the jet algorithm adopted.

We finally stress that our analytical results are also relevant for matching threshold-resummed calculations of jet cross sections to fixed-order ones. For the case of cone algorithms, based on the results of Jäger *et al.* [12], this was already exploited in Ref. [19]. Our present calculation allows to extend this procedure to the case of the nowadays more popular k_t-type algorithms. We note that the jets we consider here remain massive near partonic threshold (see the discussion in Ref. [19]), which affects the logarithmic structure of the partonic cross sections [34] and corresponds to the situation encountered in experiment and in the "exact" NLO codes such as FastNLO and FastJet. It is known [35] that "nonglobal" threshold logarithms arise in this case, since the observable is sensitive to radiation into only a limited part of phase space. These appear first at next-to-leading logarithmic level.

ACKNOWLEDGMENTS

We are grateful to G. Soyez for providing results from his FastJet code and for helpful comments. We also thank R. Fatemi and C. Gagliardi for stimulating our interest in the topic discussed in this paper. A. M. thanks the Alexander von Humboldt Foundation, Germany, for support through a Fellowship for Experienced Researchers. W. V. is grateful to Brookhaven National Laboratory for its hospitality during the completion of this work.

[1] L. Adamczyk *et al.* (STAR Collaboration), Phys. Rev. D **86**, 032006 (2012); B. I. Abelev *et al.* (STAR Collaboration), Phys. Rev. Lett. **100**, 232003 (2008); P. Djawotho (STAR Collaboration), J. Phys. Conf. Ser. **295**, 012061 (2011).
[2] For a brief review, see, G. Soyez, Nucl. Phys. B, Proc. Suppl. **191**, 131 (2009).
[3] S. D. Ellis and D. E. Soper, Phys. Rev. D **48**, 3160 (1993).
[4] S. Catani, Y. L. Dokshitzer, M. H. Seymour, and B. R. Webber, Nucl. Phys. **B406**, 187 (1993), and references therein.
[5] Y. L. Dokshitzer, G. D. Leder, S. Moretti, and B. R. Webber, J. High Energy Phys. 08 (1997) 001.
[6] M. Cacciari, G. P. Salam, and G. Soyez, J. High Energy Phys. 04 (2008) 063.
[7] See, for example, G. C. Blazey *et al.*, arXiv:hep-ex/0005012, and references therein.
[8] B. I. Abelev *et al.* (STAR Collaboration), Phys. Rev. Lett. **97**, 252001 (2006). For jet studies for the k_t and anti-k_t algorithms at STAR, see, Ref. [33].
[9] M. H. Seymour, Nucl. Phys. **B513**, 269 (1998).
[10] G. P. Salam and G. Soyez, J. High Energy Phys. 05 (2007) 086.

[11] D. de Florian, S. Frixione, A. Signer, and W. Vogelsang, Nucl. Phys. **B539**, 455 (1999).
[12] B. Jäger, M. Stratmann, and W. Vogelsang, Phys. Rev. D **70**, 034010 (2004).
[13] G. F. Sterman and S. Weinberg, Phys. Rev. Lett. **39**, 1436 (1977).
[14] M. Furman, Nucl. Phys. **B197**, 413 (1982).
[15] F. Aversa, P. Chiappetta, M. Greco, and J. P. Guillet, Nucl. Phys. **B327**, 105 (1989).
[16] F. Aversa, M. Greco, P. Chiappetta, and J. P. Guillet, Z. Phys. C **46**, 253 (1990).
[17] D. de Florian, R. Sassot, M. Stratmann, and W. Vogelsang, Phys. Rev. Lett. **101**, 072001 (2008); Phys. Rev. D **80**, 034030 (2009).
[18] J. Kapitan (STAR Collaboration), arXiv:1111.1892; E. Bruna (STAR Collaboration), AIP Conf. Proc. **1422**, 190 (2012).
[19] D. de Florian and W. Vogelsang, Phys. Rev. D **76**, 074031 (2007).
[20] S. D. Ellis, C. K. Vermilion, J. R. Walsh, A. Hornig, and C. Lee, J. High Energy Phys. 11 (2010) 101.
[21] J. P. Guillet, Z. Phys. C **51**, 587 (1991).
[22] B. Jäger, A. Schäfer, M. Stratmann, and W. Vogelsang, Phys. Rev. D **67**, 054005 (2003).
[23] T. Kluge, K. Rabbertz, and M. Wobisch, arXiv:hep-ph/0609285; M. Wobisch *et al.* (fastNLO Collaboration), arXiv:1109.1310; see also online tool at http://fastnlo.hepforge.org/form/index.html.
[24] Z. Nagy, Phys. Rev. Lett. **88**, 122003 (2002); Phys. Rev. D **68**, 094002 (2003).
[25] P. M. Nadolsky, H.-L. Lai, Q.-H. Cao, J. Huston, J. Pumplin, D. Stump, W.-K. Tung, and C.-P. Yuan, Phys. Rev. D **78**, 013004 (2008).
[26] M. Cacciari, G. P. Salam, and G. Soyez, Eur. Phys. J. C **72**, 1896 (2012); M. Cacciari and G. P. Salam, Phys. Lett. B **641**, 57 (2006).
[27] G. Soyez (private communication).
[28] A. Abulencia *et al.* (CDF Collaboration), Phys. Rev. D **75**, 092006 (2007); Phys. Rev. D **75**, 119901(E) (2007).
[29] T. Aaltonen *et al.* (CDF Collaboration), Phys. Rev. D **78**, 052006 (2008); Phys. Rev. D **79**, 119902(E) (2009).
[30] S. Chatrchyan *et al.* (CMS Collaboration), Phys. Rev. Lett. **107**, 132001 (2011).
[31] G. Aad *et al.* (ATLAS Collaboration), Phys. Rev. D **86**, 014022 (2012).
[32] G. Soyez, Phys. Lett. B **698**, 59 (2011).
[33] M. Ploskon (STAR Collaboration), Nucl. Phys. **A830**, 255c (2009).
[34] N. Kidonakis, G. Oderda, and G. F. Sterman, Nucl. Phys. **B525**, 299 (1998).
[35] A. Banfi, M. Dasgupta, and Y. Delenda, Phys. Lett. B **665**, 86 (2008); C. W. Bauer, N. D. Dunn, and A. Hornig, Phys. Rev. D **82**, 054012 (2010); see also, M. Dasgupta and G. P. Salam, Phys. Lett. B **512**, 323 (2001); J. High Energy Phys. 03 (2002) 017; C. F. Berger, T. Kucs, and G. F. Sterman, Phys. Rev. D **65**, 094031 (2002); A. Banfi and M. Dasgupta, J. High Energy Phys. 01 (2004) 027.